RESEARCH Open Access

Zinc finger DHHC-type palmitoyltransferase 13-mediated S-palmitoylation of GNA13 from Sertoli cell-derived extracellular vesicles inhibits autophagy in spermatogonial stem cells

Heran Cao^{1,2†}, Huihui Gao^{1,3,4†}, Yan Li^{1,2}, Long Li¹, Shujuan Liu¹, Tianqi Jin¹, Yang Wang¹, Ye Gong¹, Shuiqiao Yuan⁴ and Wuzi Dong^{1,2*}

Abstract

Extracellular vesicles (EVs) originating from testicular somatic cells act as pivotal intermediaries in cell signaling cross-talk between spermatogenic cells and the testicular microenvironment. The intricate balance between palmitoylation and depalmitoylation governs the positioning of protein cargos on the membrane, thereby influencing cellular activities by concentrating these proteins in EVs for delivery to recipient cells. Here, we reveal that GNA13 undergoes specific S-palmitoylation at Cys14 and Cys18 residues in Sertoli cells (SCs), a modification essential for its localization to the plasma membrane. We identify DHHC13, a member of the zinc finger DHHC-type palmitoyltransferase family that catalyzes protein S-palmitoylation, as the enzyme responsible for this critical post-translational modification. Additionally, GNA13 palmitoylation is indispensable for its selective enrichment in EVs emanating from SCs. Intriguingly, we discovered the presence of palmitoylated GNA13 in SC-derived EVs significantly downregulates autophagy levels in spermatogonial stem cells (SSCs), and the inhibition of GNA13 palmitoylation attenuates its interaction with ARHGEF12 which leads to diminished RhoA activity and consequent elevation of autophagy in SSCs. Our results illuminate the crucial role of DHHC13-mediated GNA13 S-palmitoylation in modulating autophagy levels in SSCs through SCs-derived EVs, suggesting that PM-GNA13-EV may serve as a potential candidate for further exploration in addressing fertility-related challenges during spermatogenesis.

Keywords GNA13, Palmitoylation, Sertoli cells, Extracellular vesicles, Autophagy, Spermatogonial stem cells

*Correspondence:

Wuzi Dong

dongwuzi@nwafu.edu.cn

Introduction

In the mammalian spermatogenic microenvironment, Sertoli cells act as coordinators, providing structural support and nourishment to germ cells during spermatogenesis [1]. Extracellular vesicles (EVs), ubiquitously secreted nanoscale membrane-bound entities, are capable of ferrying an assortment of biomolecules—including proteins, lipids, mRNA, and microRNA—thus serving as key mediators in intercellular communication and biological regulation [2–5]. Recent advances have enabled the isolation and characterization of Sertoli cell-derived EVs, revealing their instrumental roles in the preservation



© The Author(s) 2025. **Open Access** This article is licensed under a Creative Commons Attribution-NonCommercial-NoDerivatives 4.0 International License, which permits any non-commercial use, sharing, distribution and reproduction in any medium or format, as long as you give appropriate credit to the original author(s) and the source, provide a link to the Creative Commons licence, and indicate if you modified the licensed material. You do not have permission under this licence to share adapted material derived from this article or parts of it. The images or other third party material in this article are included in the article's Creative Commons licence, unless indicated otherwise in a credit line to the material. If material is not included in the article's Creative Commons licence and your intended use is not permitted by statutory regulation or exceeds the permitted use, you will need to obtain permission directly from the copyright holder. To view a copy of this licence, visit http://creativecommons.org/licenses/by-nc-nd/4.0/.

[†]Heran Cao and Huihui Gao contributed equally to this work.

¹ College of Animal Science and Technology, Northwest A&F University, No. 3 Taicheng Road, Yangling, Shaanxi 712100, P. R. China

² Key Laboratory of Animal Genetics, Breeding and Reproduction of Shaanxi Province, College of Animal Science and Technology, Northwest A&F University, Yangling 712100, China

³ Department of Obstetrics and Gynecology, The Central Hospital of Wuhan, Tongji Medical College, Huazhong University of Science and Technology, Wuhan 430014, China

⁴ Institute of Reproductive Health, Tongji Medical College, Huazhong University of Science and Technology, Wuhan 430030, China

of testicular spermatogenesis [6–8]. Specifically, within the seminiferous tubules, these EVs have been found to carry MicroRNA- 486 - 5p, a critical factor that promotes the differentiation of spermatogonial stem cells (SSCs) [9]. Our latest study further corroborates the protective effects of EVs, demonstrating that small RNAs within EVs derived from mouse Sertoli cells effectively mitigate SSC apoptosis [10]. While post-translational modifications (PTMs) of proteins encapsulated within EVs are emerging as promising biomarkers for various clinical applications [11–13], the repertoire and functional significance of PTMs in Sertoli cell-derived EVs during spermatogenesis remain largely unexplored.

S-palmitoylation is a dynamic and reversible posttranslational lipid modification characterized by the covalent attachment of a 16-carbon palmitic acid moiety to cysteine residues via labile thioester bonds. This enzymatic process is chiefly mediated by palmitoyl acyltransferases (PATs), which are defined by their signature DHHC (Asp-His-His-Cys) motif. Through modulating membrane affinity or protein conformation, S-palmitoylation exerts a profound influence on a range of cellular activities, including protein-membrane interactions, intracellular trafficking, stability, and protein-protein interactions [14-17]. Accumulating evidence increasingly emphasizes the critical function of palmitoylated proteins in the regulation of male spermatogenesis. The abnormal palmitoylation disorder plays a key role in the destruction of blood-testis barrier (BTB), the blocking of autophagy degradation, and the abnormality and apoptosis of sperm during spermatogenesis [18-21]. Recent studies also spotlight the heterogeneity in the composition of palmitoylated proteins within EVs originating from differently sized prostate cancer cells [22]. Additionally, the palmitoylation of Alix, a well-established EV marker, is implicated in the preservation of vesicular architecture [23]. Remarkably, the palmitoylation of ACE2, localized on the surface of EVs, has been shown to confer protective effects against SARS-CoV- 2-induced pulmonary inflammation [24].

Guanine nucleotide binding protein, alpha 13 (GNA13), also known as $G\alpha13$, is a key α -subunit of heterotrimeric G proteins, responsible for mediating signal transduction from G protein-coupled receptors (GPCRs) [25]. Its expression is ubiquitous across various tissues, encompassing liver [26], lymphatic system [27], and testes [28]. In the context of human spermatogenesis, GNA13 not only contributes to the process but also undergoes nuclear translocation, underscoring its multifaceted role [28]. Although GNA13 in EVs has been reported in breast cancer cells [29], whether it plays a role in EVs of testicular cells remains unknown. Intriguingly, recent discoveries have highlighted the capability of

GNA13 to modulate the expression of BCL2 in germinal center B-cell-like diffuse large B-cell lymphoma (GCB-DLBCL) cells, and this regulatory activity is contingent on its palmitoylation status [30].

In this study, we elucidate the functional role of GNA13 S-palmitoylation at Cys14 and Cys18 residues within mouse Sertoli cells, a modification crucial for its plasma membrane localization. We identify DHHC13 as the key palmitoyl acyltransferase responsible for this posttranslational modification. Intriguingly, the palmitoylated form of GNA13 is selectively enriched in EVs released by Sertoli cells and acts as a modulator of autophagy levels in SSCs. We further demonstrate that inhibition of GNA13 palmitoylation compromises its interaction with ARH-GEF12, leading to a subsequent decline in RhoA activity and elevated autophagy in SSCs. Our findings shed light on the complex interplay between DHHC13-mediated GNA13 palmitoylation and autophagy regulation in SSCs via SCs-derived EVs, offering novel mechanistic insights into spermatogenesis. These discoveries also contribute to a deeper understanding of the pathological basis and potential therapeutic strategies for male infertility linked to aberrant palmitoylation levels.

Results

Collection and identification of extracellular vesicles from primary mouse sertoli cells

Mouse Sertoli cells (SCs) were isolated and purified at the pubertal stage, specifically at 3 weeks postpartum. The expression of SC-specific markers, GATA4 and SOX9, was confirmed through immunodetection (Figs. 1A and B). Extracellular vesicles (EVs) were harvested from the conditioned medium of SCs, which was pre-cleared of EVs. Scanning electron microscopy revealed that these SCs-derived EVs exhibited a consistent morphology, with a characteristic diameter of approximately 50-100 nm (Fig. 1C). Nanoparticle tracking analysis (NTA) further corroborated these findings, demonstrating that the majority of EVs fell within the size range of 50–100 nm, with a peak in the diameter distribution at 96 nm (Fig. 1D). Western blot analysis was conducted to validate the presence of canonical EVs markers, including CD63, HSP70, and ALIX (Fig. 1E).

The palmitoylation inhibitor 2-BP alters the protein distribution in extracellular vesicles from mouse sertolicals

To more definitively ascertain the presence of protein palmitoylation in SCs-derived EVs, we performed a proteomic analysis on both native and 2-bromopalmitate (2-BP)-treated EVs harvested from primary mouse SCs. Initially, we employed lentiviral vectors carrying specific palmitoylation modification sites to infect primary SCs.

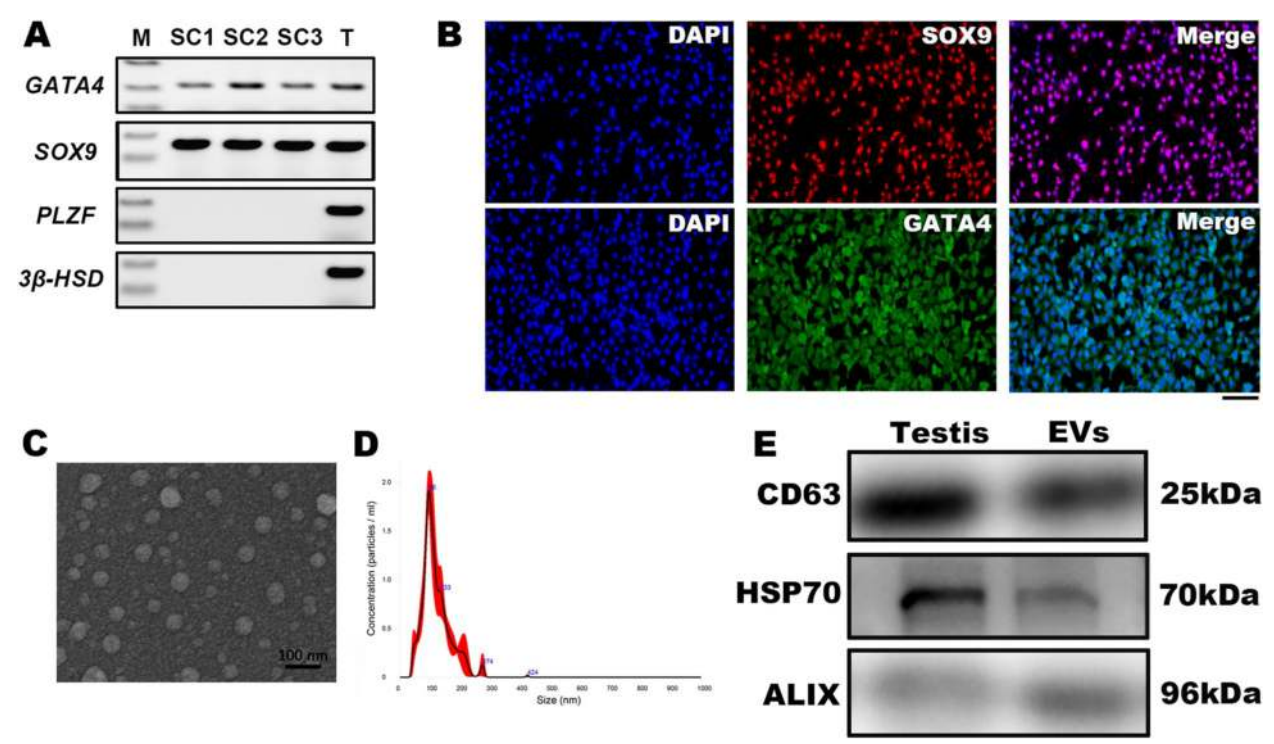


Fig. 1 Separation and identification of extracellular vesicles derived from mouse primary Sertoli cells. **A** The Sertoli cells (SCs) purity was verified by PCR assay for the detection of *GATA4*, *SOX9*, *PLZF*, and *3β-HSD* gene expression. **B** Detection of the expression of SCs-related markers SOX9 and GATA4 by immunofluorescence. Scale bar, 100 μm. **C** Observation of extracellular vesicles (EVs) morphology through scanning electron microscope (SEM). **D** Hydrodynamic size distribution of SCs-derived EVs measured by NanoSight. **E** WB of testis and EVs fractions blotted with antibodies raised against membrane EV-positive marker CD63 and cytosolic EV-positive markers (HSP70 and ALIX)

Under the influence of 125 µM of 2-BP, we observed a significant retention of red fluorescence in the cellular cytoplasm (Fig. 2A). Thereafter, we utilized 4D label-free proteomics to quantify the proteomes of SCs and their corresponding EVs, both in control and 2-BP-treated conditions. Our analyses identified 2,724 and 2,515 proteins in the control and 2-BP-treated EVs, respectively, while 5,421 and 5,414 proteins were identified in the corresponding SCs (Supplemental Material 1). Among these, 2,148 proteins were common to all four sample types. Furthermore, a total of 2,169 proteins were concurrently identified in both control and 2-BP-treated EVs sets (Figs. 2B and C). Correlation analyses between the samples revealed a modest correlation coefficient of 0.489 between the proteomes of control and 2-BP-treated EVs (Figs. 2D and E).

Analysis of differentially expressed proteins in mouse sertoli cell-derived extracellular vesicles treated with 2-BP

To analyze differentially expressed proteins between NC (Normal Control) EVs and 2-BP-treated EVs, we identified 385 proteins with a Log2 FC >1 as listed in Supplemental Material 2. Gene Ontology (GO) enrichment analysis revealed that, in comparison to the 2-BP-treated

group, NC EVs exhibited differential expression of proteins involved in DNA replication, protein transport, and intracellular protein trafficking. Additionally, KEGG pathway enrichment highlighted differences in protein processing within the endoplasmic reticulum, proteasome function, RNA transport, splicing, endocytosis, and fatty acid metabolism (Figs. 3A and B). To assess potential palmitoylation sites, we employed GPS-Palm software to analyze the top 15 highly enriched proteins in the NC EVs. Remarkably, all 14 analyzed proteins exhibited predicted palmitoylation sites, with 10 of them showing prediction scores above 0.9. This group included the palmitoylated protein STAT3 [31] (Table S1). To validate these findings, 10 putative palmitoylated proteins were shortlisted (Table S2) and cloned into GFP-tagged expression vectors for transfection into primary SCs. Cells were then treated with 125 µM 2-BP for 24 h. Fluorescence microscopy revealed that the GFP-GNA13 control group showed membrane localization, whereas upon 2-BP treatment, GFP-GNA13 remained in the cytoplasm (Fig. 3C). The subcellular localization of the other nine proteins remained largely unchanged (Figure S1). Cell fractionation analysis also confirmed that treating TM4 cells with 2-BP significantly reduced the

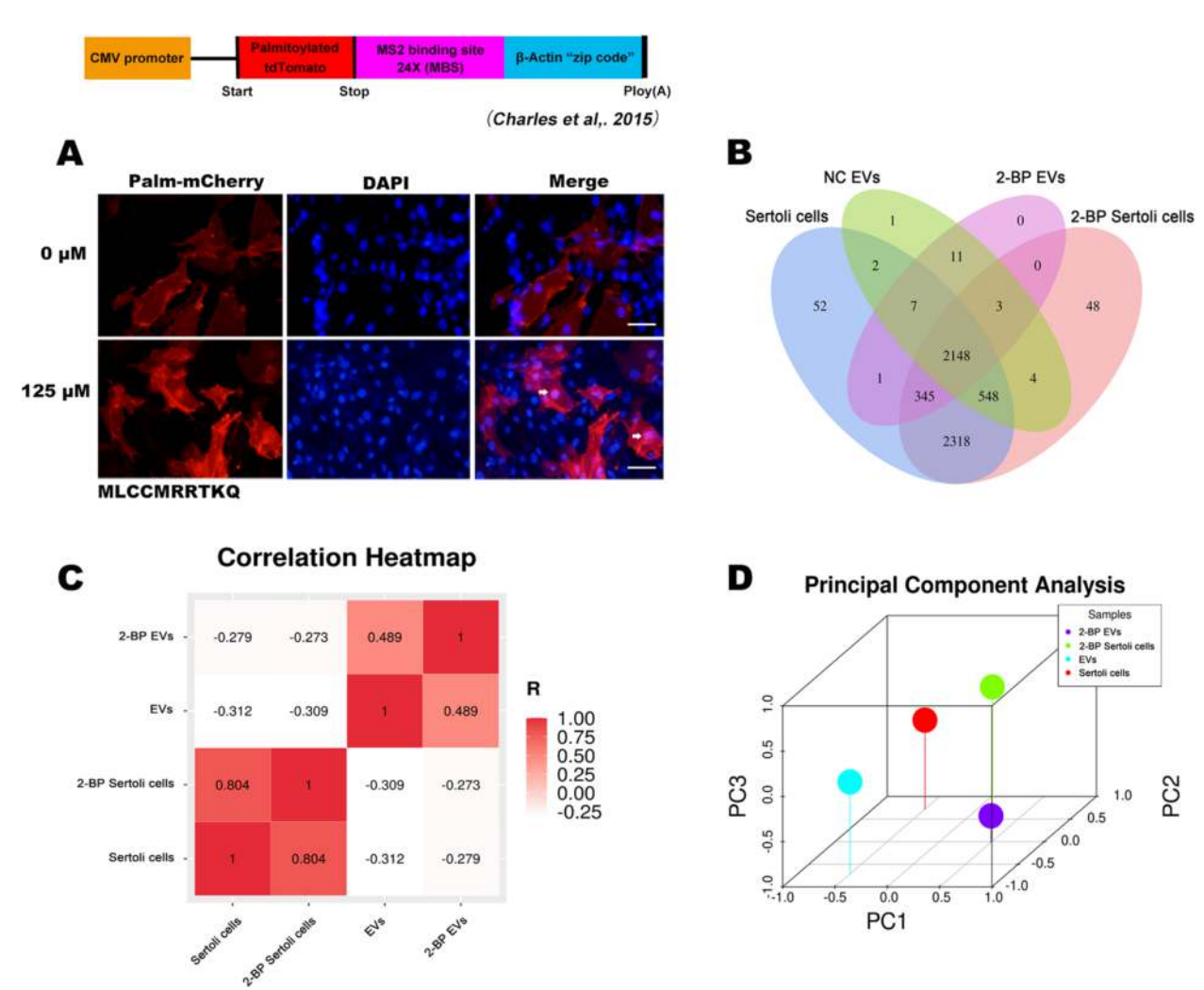


Fig. 2 The palmitoylation inhibitor 2-BP alters the expression of the proteome in Sertoli cells and their derived extracellular vesicles. **A** Treatment of primary mouse Sertoli cells (SCs) infected with palm-mCherry lentivirus with 0 μ M and 125 μ M 2-BP for 24 h. Scale bar, 50 μ m. **B** Venn diagram of the number of proteins identified in four different studies (n = 3). **C** and **D** Two-dimensional and three-dimensional principal component analysis reveal the expression patterns and correlations of four different groups of proteins (n = 3)

levels of endogenous GNA13 associated with the PM fraction, without affecting the overall GNA13 protein levels (Fig. 3D). Western blot analysis further confirmed a marked reduction in GNA13 levels in EVs from 2-BP-treated SCs compared to NC EVs (Fig. 3E). These observations suggest that palmitoylation is a key modulator of GNA13 enrichment in SCs-derived EVs.

DHHC13 mediates the palmitoylation of cysteine residues at positions 14 and 18 in GNA13

To investigate the palmitoylation status of GNA13 in primary mouse Sertoli cells, we employed an acyl-PEG exchange (APE) assay. This allowed for the isolation and semi-quantitative assessment of palmitoylated proteins. We found that endogenous GNA13 was extensively

palmitoylated, with up to 90% modification observed. The omission of hydroxylamine (HAM) treatment effectively negated this palmitoylation, suggesting that GNA13 undergoes S-palmitoylation via thioester linkages (Figs. 4A and B). We then proceeded to identify the specific cysteine residues in GNA13 that could potentially be subject to palmitoylation. Computational analysis using GPS-Palm software predicted the L-cysteine sites at positions C14, C18, and C329 as likely candidates for palmitoylation modification. To validate these predictions, HA-tagged GNA13 as well as a series of cysteine mutants (GNA13-C14S, GNA13-C18S, GNA13-C329S, GNA13-C14S/C18S, GNA13-C14S/C329S, GNA13-C18S/C329S, and GNA13-C14S/C18S/C329S) were transfected into TM4 cells (Fig. 4C). Notably, HA-GNA13

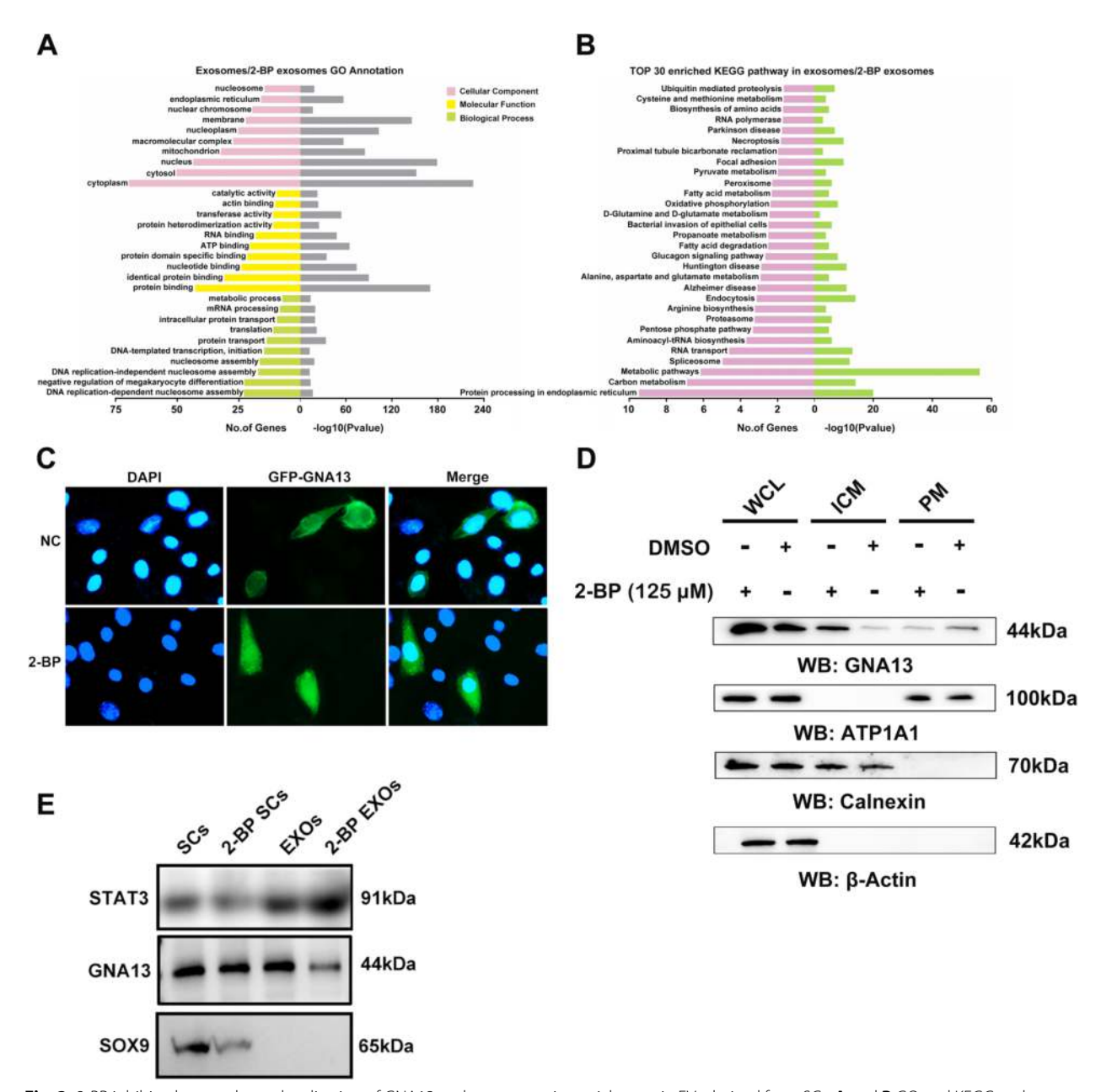


Fig. 3 2-BP inhibits the membrane localization of GNA13 and suppresses its enrichment in EVs derived from SCs. **A** and **B** GO and KEGG pathway analysis charts of differentially expressed proteins in EVs and 2-BP EVs (n=3). **C** Immunofluorescence distribution of the GFP-GNA13 in TM4 cells treated with 125 μM 2-BP for 24 h. **D** In TM4 cells expressing GNA13 and treated with 125 μM 2-BP for 24 h, the GNA13 levels in the PM and ICM were examined using Western blot. ATP1 A1, Calnexin, and β-Actin were utilized as indicators for PM, ICM, and WCL, respectively. PM plasma membrane, ICM intracellular membrane, WCL whole-cell lysate. **E** Western blot analysis of GNA13 expression in 125 μM 2-BP treated SCs and their derived EVs

localized to the cell membrane, while the GNA13-C14S and GNA13-C18S mutants were predominantly found in the nucleoplasm. Furthermore, the GNA13-C329S mutant exhibited a subtle relocalization from the membrane to the cytoplasm (Fig. 4D). Subcellular fractionation assays confirmed that transfection of TM4 cells with

the GNA13-C14S and GNA13-C18S mutants led to a significant decrease in membrane-bound GNA13 levels without affecting overall GNA13 protein expression (Fig. 4E). Using the acyl-biotinyl exchange (ABE) method, it was demonstrated that the GNA13 of C14/18S could not be palmitoylated (Fig. 4F). This strongly suggests that

the C14 and C18 sites are the primary loci for palmitoylation modification in GNA13. The palmitoylation of proteins is catalyzed by the DHHC family of palmitoylation modifiers [32]. The proteomic analysis revealed that six palmitoyl acyltransferases (PATs)—DHHC5, DHHC6, DHHC13, DHHC17, DHHC20, and DHHC21—are expressed in primary mouse SCs, as detailed in Table S3. Co-immunoprecipitation (Co-IP) assays showed that when HA-tagged GNA13 was co-transfected with any of the six Flag-tagged PATs into TM4 cells, a specific interaction between GNA13 and DHHC13 was observed (Fig. 4G). Furthermore, the reconstituted expression of GNA13-C14S and GNA13-C18S mutants weakened their interaction with DHHC13 (Fig. 4H).

The palmitoylated GNA13 carried in sertoli cell-derived extracellular vesicles inhibits the autophagy of spermatogonial cells

To further explore the role of GNA13 palmitoylation in EVs enrichment, we collected exosomes from TM4 cells transfected with either HA-tagged GNA13 or its palmitoylation-deficient mutants HA-GNA13-C14S/C18S. Western blot analysis revealed a substantial decrease in HA levels in EVs from TM4 cells transfected with HA-GNA13-C14S/C18S, compared to those transfected with WT-GNA13 (Fig. 5A). We then exposed primary mouse SCs-derived EVs to both primary mouse spermatogonia and the C18 -4 cell line. The results showed that SCsderived EVs notably attenuated autophagy levels in both cell types (Figures S2 A and B). To assess the influence of GNA13 on autophagy in spermatogonial cells, we transfected C18 - 4 cells with GNA13-siRNA and HA-GNA13 (Figure S3). Knockdown of GNA13 led to a marked decrease in ATG5 and LC3B expression levels while increasing P62 protein levels (Figs. 5B and C), suggesting GNA13 plays a critical role in autophagy in spermatogonial cells. Subsequent transfections of HA-GNA13 into C18 -4 cells confirmed that GNA13 significantly suppressed autophagy (Figs. 5C and D). Together, these findings indicate that the palmitoylation of GNA13 not only affects its enrichment in EVs but also significantly inhibits the level of autophagy in spermatogonial cells.

The palmitoylated GNA13 binds with ARHGEF12 to promote RhoA signaling in spermatogonial cells

To explore how GNA13 regulates autophagy, we transfected C18 - 4 cells with HA-GNA13 and performed coimmunoprecipitation (Co-IP) assays using HA-specific antibodies. Silver staining revealed differential protein enrichment profiles between the experimental and control groups (Fig. 6A). Proteomic analysis identified 373 proteins in the IgG control group and 541 proteins in the HA-targeted group; among these, 219 proteins were uniquely enriched in the HA group (Figs. 6B and C). A combined analysis using STRING database and our proteomic data highlighted three key interacting proteins: ARHGDIA, ARHGEF12, and GNB1 (Figs. 6D and E). It is well-established that RhoA operates as a downstream effector in G-protein-coupled receptor pathways linked to GNA13 [33]. RhoA has also been implicated in the regulation of autophagy [34]. Notably, ARHGEF12 has a strong association with the RhoA signaling pathway. Co-IP assays confirmed a direct interaction between GNA13 and ARHGEF12, and this interaction was significantly diminished when the GNA13-C14S/C18S mutant was employed (Fig. 6F). Immunofluorescence assays further corroborated the reduced affinity between the GNA13-C14S/C18S mutant and ARHGEF12 in C18 -4 cells (Fig. 6G). Subsequent Western blot analysis showed that while wild-type GNA13 elevated the expression levels of RhoA in C18 -4 cells, the GNA13-C14S/C18S mutant had no discernible impact on RhoA expression (Fig. 6H).

(See figure on next page.)

Fig. 4 DHHC13 palmitoylates GNA13 at Cys14 and Cys18 to maintain GNA13 PM localization. **A** Palmitoylation of GNA13 was analyzed by ABE and Western blot in SCs. The presence or absence of hydroxylamine (HAM) during the reaction was used as a control for reaction specificity. Western blot analysis with streptavidin-beads pulldown is shown depicting the banding pattern of S-palmitoylated GNA13. **B** APE assay was performed to analyze the GNA13 palmitoylation in SCs. The top band indicates the palmitoylated GNA13 (PEG-GNA13). **C** Information on point mutation vectors for the GNA13 protein. **D** In TM4 cells expressing either WT-HA-GNA13 or GNA13-C14/18S, Western blot was employed to examine GNA13 levels within PM and ICM fractions. ATP1 A1, Calnexin, and β-Actin were utilized as indicators for PM, ICM, and WCL respectively. PM plasma membrane, ICM intracellular membrane, WCL whole-cell lysate. **E** TM4 cells with reconstituted expression of WT-HA-GNA13 or GNA13-C14/18S were incubated with Goat Anti-Mouse Alexa Fluor 594. GNA13 cellular localization was visualized by immunofluorescent staining using an antibody against HA. Scale bar, 25 μm. **F** TM4 cells with reconstituted expression of WT-HA-GNA13 or GNA13-C14/18S were treated with 125 μM 2-BP for 24 h. Palmitoylation levels of GNA13 were analyzed by ABE assay. Western blot analysis with streptavidin-beads pulldown is shown depicting the banding pattern of S-palmitoylated GNA13. **G** Immunoprecipitation (with an anti-HA antibody) and immunoblot analysis of TM4 cells transfected with plasmids encoding WT-HA-GNA13 and Flag-DHHC5, Flag-DHHC13, Flag-DHHC17, Flag-DHHC20 or Flag-DHHC21 for 24 h. **H** TM4 cells with reconstituted expression of Flag-DHHC13 and WT-HA-GNA13 or GNA13-C14/18S for 24 h. Palmitoylation levels of GNA13 were analyzed by ABE assay. Western blot analysis with streptavidin-beads pulldown in the absence or presence of HAM is shown depicting the banding pattern of S-palmitoylated GNA13

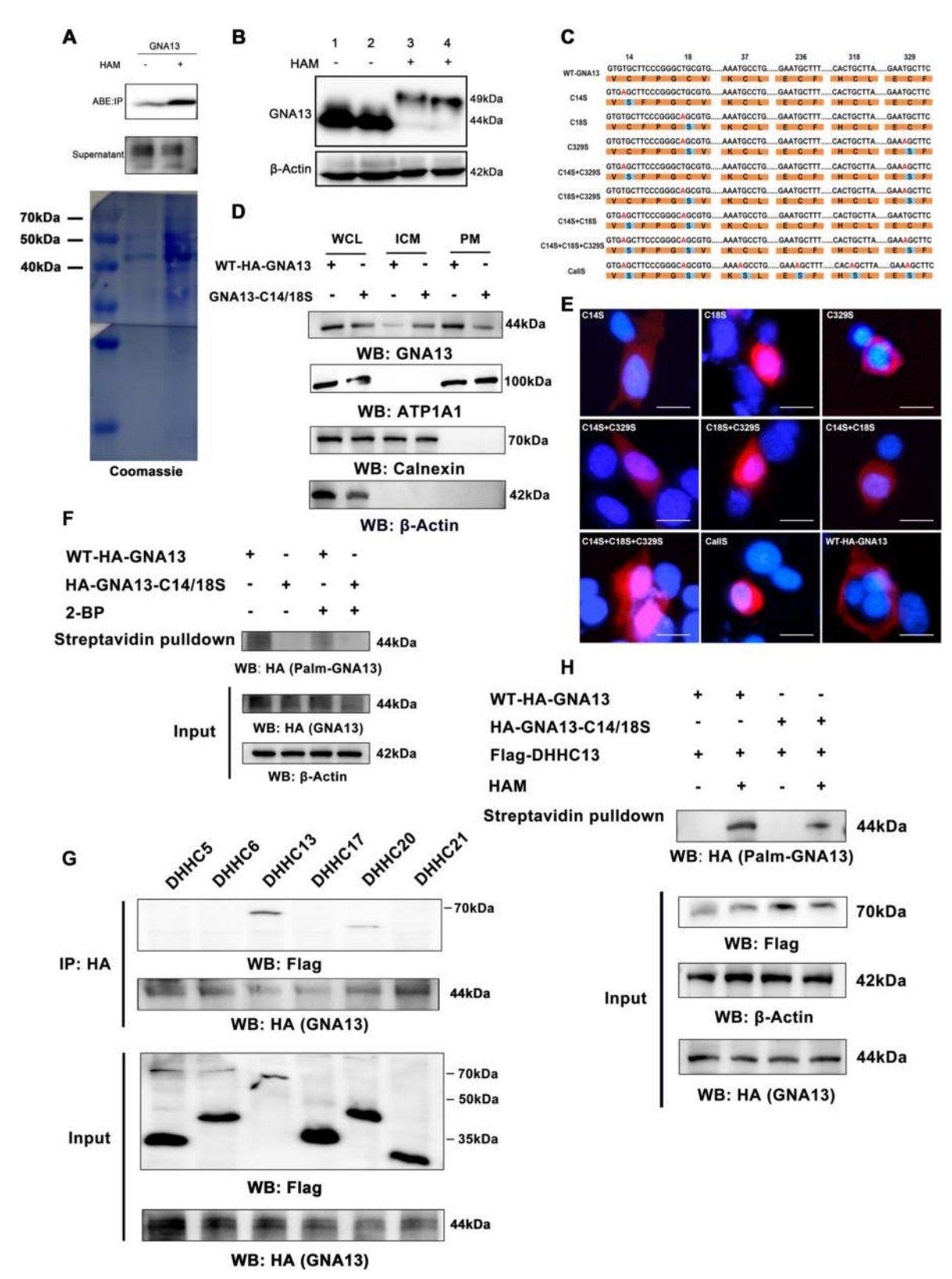


Fig. 4 (See legend on previous page.)

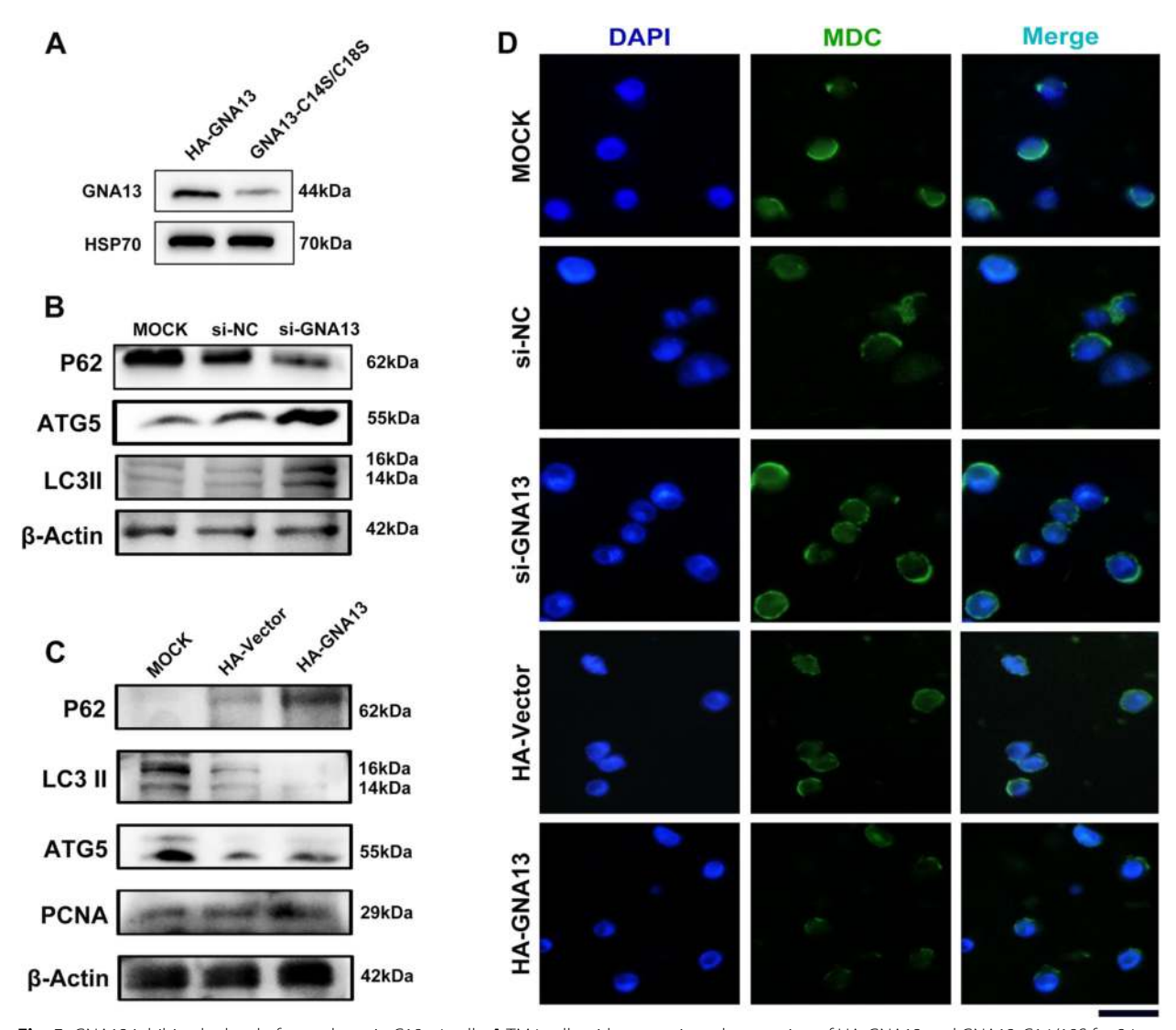


Fig. 5 GNA13 inhibits the level of autophagy in C18 -4 cells. **A** TM4 cells with reconstituted expression of HA-GNA13 and GNA13-C14/18S for 24 h. GNA13 protein levels in TM4 cells-derived EVs were assessed by Western blot. **B** Western blot analysis was performed to determine changes of autophagic molecules when GNA13 knockdown (si-GNA13) or control non-specific siRNA (si-NC) were transfected in C18 -4 cells for 24 h. **C** Western blot analysis was performed to determine changes of autophagic molecules when GNA13 overexpressed (HA-GNA13) or empty vector (HA-Vector) were transfected in C18 -4 cells for 24 h. **D** MDC stained vesicles were visualized in HA-GNA13 or HA-Vector, and si-GNA13 or si-NC were transfected in C18 -4 cells for 24 h. Scale bar, 25 μm

Discussion

Testicular somatic cell-derived extracellular vesicles (EVs) are gaining recognition as pivotal mediators of cellular signaling cross-talk between spermatogonial cells and the testicular microenvironment [6]. These EVs originating from Sertoli cells have been shown to orchestrate spermatogenesis through the transfer of miRNAs and proteins [8]. Notably, these EVs have been implicated in processes such as spermatogonial stem cells (SSCs) differentiation [9] and proliferation [35]. In this study, we substantiate the inhibitory role of GNA13, enriched in

EVs from Sertoli cells, in regulating autophagy levels in spermatogonial cells. The enrichment of GNA13 in EVs is predominantly mediated by its palmitoylation modification. Additionally, DHHC13 within Sertoli cells (SCs) catalyzes the palmitoylation of GNA13 at the position 14 and 18 cysteine residues. Impeding palmitoylation of GNA13 leads to reduced content of GNA13 in EVs. Notably, the GNA13-mediated regulation of spermatogonial cell autophagy relies on the interaction between palmitoylated GNA13 and ARHGEF12, activating RhoA expression.

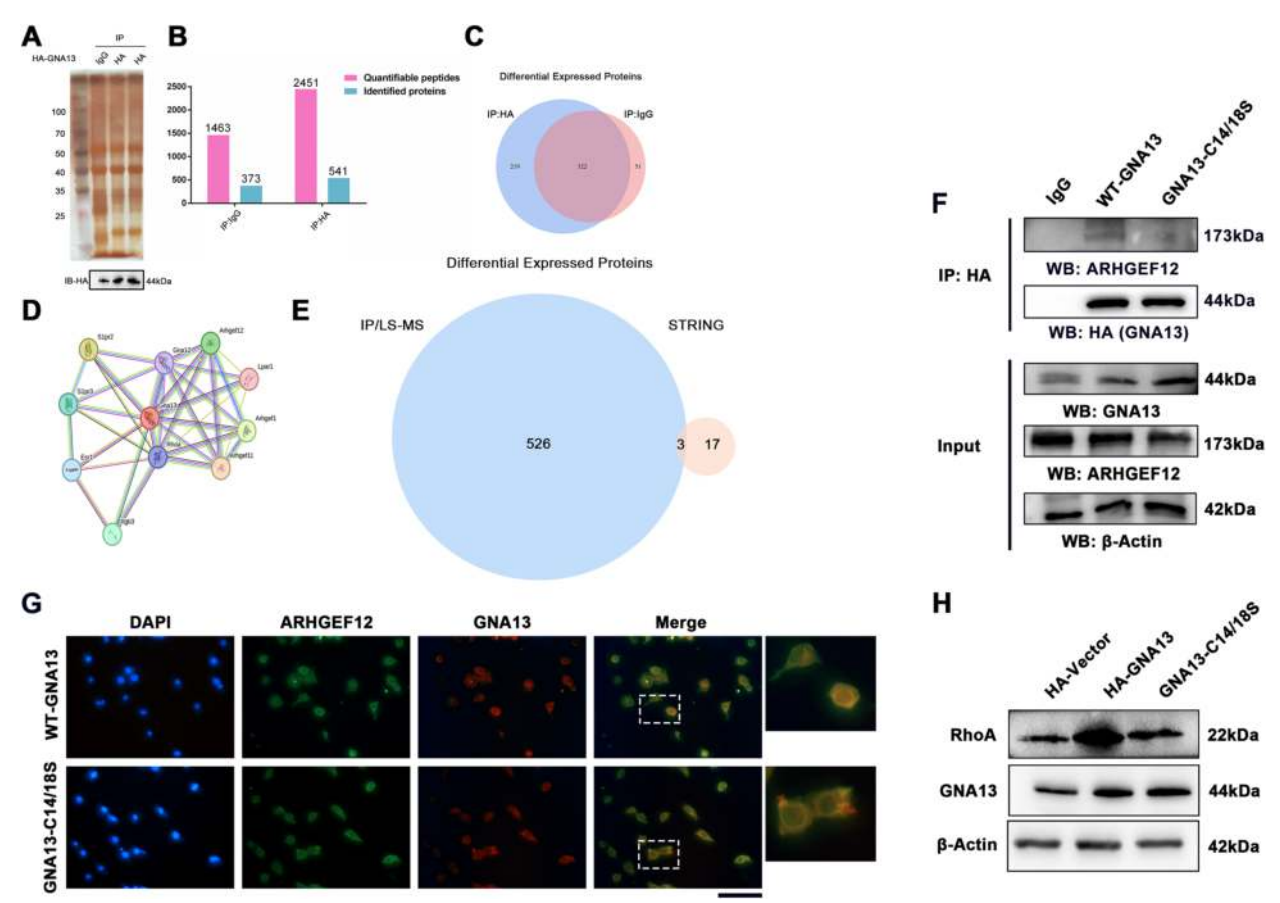


Fig. 6 Palmitoylated GNA13 promotes the expression of RhoA protein in C18 -4 cells by binding to ARHGEF12. **A** C18 -4 cells transfected with control vector or HA-GNA13 were lysed, anti-HA antibody was used for immunopurification, and irrelevant IgG was used for control. We used mass spectrometry to analyze protein bands that were acquired by dealing with eluent with silver staining. Some binding proteins were verified in C18 -4 cells. **B** and **C** Differential enrichment analysis of HA and IgG groups in Co-IP pull-down assay. **D** and **E** Interactive analysis of STRING data and Co-IP mass spectrometry results. **F** C18 -4 cells transfected with WT-GNA13 and GNA13-C14/18S for 24 h. Whole cell lysates (WCL) were used for Co-IP and western blotting with anti-HA and irrelevant IgG (Control). **G** Representative images of GNA13 immunostaining colocalization with ARHGEF12 in C18 -4 cells with transfecting WT-GNA13 and GNA13-C14/18S for 24 h. Scale bars, 50 µm. **H** Western blot analysis was performed to determine changes of RhoA when WT-GNA13 or GNA13-C14/18S were transfected in C18 -4 cells for 24 h

Membrane localization plays a pivotal role in sorting cargo into EVs [36]. The membrane localization of protein cargo relies on dynamic regulation of palmitoylation and depalmitoylation [37-40]. To investigate whether cargo within EVs derived from SCs is associated with protein palmitoylation modifications, we observed profound changes in the protein spectrum of SCs-derived EVs upon treatment with the palmitoylation inhibitor 2-bromopalmitate (2-BP). Although our Sertoli cell isolation protocol achieved >95% purity, a minor presence of other testicular cell types cannot be entirely ruled out. However, the proteomic analysis focused on EVs derived specifically from Sertoli cells, as evidenced by the enrichment of SC-specific marker SOX9. Additionally, stringent criteria (Log2 FC > 1) were applied to filter out proteins potentially contributed by non-target cells. Intriguingly, the current study revealed that under 2-BP treatment, GFP-GNA13 localization underwent a significant shift from the plasma membrane to the cytoplasm, which is consistent with previous report by Xia et al. [30] Additionally, we observed a substantial reduction in the enrichment of GNA13 within SCs-derived EVs following 2-BP treatment. These findings indicate that palmitoylation regulates the secretion of GNA13 in EVs. Utilizing acyl-biotin exchange (ABE) assays, we confirmed that GNA13 can be strongly palmitoylated at Cys14 and Cys18 residues. Moreover, the substitution of serine for the Cys14 and Cys18 residues eliminated the palmitoylation of GNA13, leading to a disruption in its membrane localization and reduced secretion into EVs. Additionally, we identified the palmitoyl transferase DHHC13 as the enzyme responsible for the palmitoylation of GNA13. Given recent evidence suggesting that the enrichment of palmitoylation in exosomes impacts various physiological

and pathological processes [22, 24, 41, 42], the role of GNA13 within SCs-derived EVs cannot be overlooked in its impact on SSCs.

Autophagy plays a critical role in the proliferation, differentiation, meiotic progression, and spermatogenesis of SSCs [43-45]. EVs exert an influence on autophagy levels in target cells through the transfer of miRNAs and protein cargo [46–49]. In our previous research, we demonstrated that miR- 10b derived from EVs originating from mouse SCs inhibits apoptosis in primary spermatogonial cells [10]. In the current study, we discovered that treatment of in vitro cultured SSCs with EVs derived from SCs significantly suppresses their autophagy levels, which expanded the view of the functions of EVs in SSCs. Moreover, we found that inhibiting the expression of GNA13 substantially enhances autophagy and GNA13 significantly inhibit autophagy levels in C18 -4 cells. This suggests that palmitoylation-modified GNA13 not only affects its enrichment in exosomes but also participates in regulating autophagy in spermatogonial cells. We further identified an interaction between GNA13 and ARHGEF12, a guanine nucleotide exchange factor (GEF) that specifically activates RhoA by promoting the exchange of GDP for GTP. ARHGEF12, also known as LARG (leukemia-associated RhoGEF), is a critical mediator of G protein-coupled receptor (GPCR) signaling, linking extracellular signals to intracellular RhoA activation. Our data demonstrate that inhibiting the palmitoylation of GNA13 significantly suppresses its binding to ARH-GEF12, indicating that this interaction is dependent on GNA13's palmitoylation status. RhoA, a small GTPase and proximal downstream effector of GNA13 [50], is a well-established regulator of autophagy [34, 51-53]. RhoA suppresses autophagy through multiple mechanisms, including the inhibition of autophagosome-lysosome fusion and the stabilization of mTORC1 signaling, a key negative regulator of autophagy. Notably, we found that wild-type GNA13 promotes RhoA protein expression in C18 -4 cells, while the palmitoylation-deficient mutant GNA13-C14S/C18S fails to do so. This suggests that palmitoylation of GNA13 within SCs-derived EVs is essential for maintaining RhoA activity, thereby suppressing autophagy in SSCs. This suggests that palmitoylation of GNA13 within SCs-derived EVs suppresses autophagy in SSCs. Palmitoylation of GNA13 appears to be essential both for its sorting into EVs and its interaction with ARHGEF12. Palmitoylation may contribute to more intricate signal interactions in the regulation of spermatogonial autophagy, thereby influencing the process of spermatogenesis.

A critical question arising from our findings is how Sertoli cell-derived EVs deliver palmitoylated GNA13 to SSCs within the complex testicular microenvironment. Sertoli cells, as polarized epithelial cells, are known to secrete EVs from both apical and basolateral domains, targeting distinct cellular niches. For instance, basolateral EV release may facilitate communication with interstitial cells or SSCs near the basement membrane, while apical secretion could directly influence germ cells within the adluminal compartment [6]. Although our study did not explicitly map EV release sites, the enrichment of palmitoylated GNA13 in EVs suggests a spatially coordinated mechanism to ensure its delivery to SSCs. Notably, EVs may bypass the BTB through pre-BTB release or transcytosis, as evidenced by the detection of Sertoli-derived exosomes in seminal fluid [54]. Importantly, even trace amounts of EV cargo can exert potent biological effects. For example, Sertoli EVs carrying miR- 486 -5p have been shown to robustly activate differentiation pathways in SSCs via PTEN downregulation [9]. Similarly, our data demonstrate that palmitoylated GNA13 in EVs suppresses SSC autophagy through RhoA activation, highlighting the functional sufficiency of EV-mediated protein transfer in modulating stem cell behavior. These observations collectively support a model wherein Sertoli cells utilize EV trafficking as a precision tool to regulate SSC homeostasis, with palmitoylation serving as a critical determinant of cargo sorting and signaling efficacy.

Conclusion

In conclusion, given the overarching implications of palmitoylation in various physiological processes and its evident role in EVs content and signaling [22–24], there's a need to delve deeper into the nuanced interactions influenced by this post-translational modification. Our research findings not only elucidate the palmitoylation-dependent mechanism of GNA13 but also provides a foundation for future studies to explore PM-GNA13-EV as a potential therapeutic avenue for fertility-related disorders. Additionally, the potential influence of EV-mediated signaling in the broader context of cell-to-cell communication in the testicular environment warrants further investigation. The challenge lies in deciphering these complex interactions and harnessing them for clinical applications.

Materials and methods

Materials

Mouse monoclonal anti-Gα13(Santa Cruz, Cat#sc-293424),Mouse monoclonal anti-CD63 (Santa Cruz,Cat#sc-5275),Rabbit polyclonal anti-Hsp70 (abcam, Cat#ab79852), Rabbit monoclonal anti-ALIX (abways, Cat#CY7215), Mouse monoclonal anti-GATA4 (Santa Cruz, Cat#sc-25310), Mouse monoclonal anti-Sox9 (Santa Cruz, Cat#sc-166505),Mouse monoclonal anti-DDDDK-Tag (ABclonal, Cat#AE005), Mouse

monoclonal anti-HA-Tag (ABclonal, Cat#AE008), Rabbit monoclonal anti-BAX (abways, Cat#CY5059), Rabbit monoclonal anti-Bcl- 2 (abways, Cat# CY5032), Rabbit monoclonal anti-Cleaved Caspase- 3 (CST, Cat#9664), Rabbit monoclonal Anti-SQSTM1/p62 (PTM BIO, Cat#PTM- 6434), Rabbit monoclonal Anti-LC3II(PTM BIO, Cat#PTM- 6384), Mouse monoclonal anti-STAT3 (Santa Cruz, Cat#sc- 293151),Rabbit monoclonal Anti-Rho A (abways, Cat#CY5640), Rabbit polyclonal anti-ARHGEF12 (proteintech, Cat#22,441-1-AP), Rabbit monoclonal Anti-ATP1 A1 (PTM BIO, Cat#PTM- 6271), Rabbit monoclonal Anti-Calnexin (abways, Cat#CY5839), Mouse monoclonal anti-beta Actin (abways, Cat#AB0011). All antibodies were incubated overnight at 4 °C unless otherwise specified. HRP-labeled Goat Anti-Rabbit IgG(H +L) (Beyotime, Cat#A0208), HRP-labeled Goat Anti-Mouse IgG(H +L) (Beyotime, Cat#A0216), Goat Anti-Rabbit IgG (H +L) Alexa Fluor 488 (abways, Cat#AB0141), Goat Anti-Rabbit IgG (H +L) Alexa Fluor 594 (abways, Cat#AB0151), Goat Anti-Mouse IgG (H + L) Alexa Fluor 488 (abways, Cat#AB0142), Goat Anti-Mouse IgG (H +L) Alexa Fluor 594 (abways, Cat#AB0152); 2-Bromopalmitate (2-BP) (MilliporeSigma, Cat#21604), N-ethylmaleimide (NEM) (Thermo Scientific™, Cat#23030), BeyoMag™ Streptavidin Magnetic Beads (Beyotime, Cat#P2151), NH2OH Dimethylsulfoxide (Merck, Cat#467804), (DMSO) (Sigma-Aldrich, Cat#D2650), KnockOut SR Medium (Thermo Scientific™, Cat#10828028),DMEM high glucose (HyClone, Cat#SH30243.01B), fetal bovine serum (FBS) (zeta-life, Cat#Z7010 FBS- 500), Penicillin-Streptomycin Liquid (Solarbio, Cat#P1400), Lipofectamine™ 3000 (Invitrogen, Cat#L3000015), DMEM/F-(HyClone, Cat#SH30023.01B), collagenase type IV (Sigma-Aldrich, Cat#C5138 -25MG), 2× RealStar Power SYBR qPCR Mix (GenStar, Cat#A311), Immobilon® UltraPlus Western HRP Substrate (Millipore, Cat#WBULP- 20ML), phosphate-buffered saline (PBS) (Hyclone, Cat#SH30256.LS), Protease Inhibitor Cocktail (100X) (CST, Cat#5871), Trizol (Beyotime, Cat#R0016), RIPA Lysis Buffer (MedChemExpress, Cat#HY-K1001), DAPI (Beyotime, Cat#C1005), Bovine Serum Albumin (BSA) (Sigma-Aldrich, Cat#V900933), HBSS (Solarbio, Cat#H1025).

Animals and ethical statement

A total of 30 ICR mice (5–7 days old) were obtained from the Laboratory Animal Center of Northwest A&F University (Yangling, China). Mice were euthanized by cervical dislocation under deep anesthesia induced via intraperitoneal injection of sodium pentobarbital (100 mg/kg body weight). The care and use of experimental animals completely conformed to the university animal

welfare laws, guidelines, and policies. All experimental procedures were approved by the Institutional Animal Care and Use Committee of Northwest A&F University in China.

Cell culture and plasmid construction

Adult mice were obtained from an approved animal facility and were euthanized them using an approved method. Sterilize surgical tools with ethanol and sterile water. Make a midline incision on the scrotum to expose the testes, then excise and transfer them to a Petri dish containing chilled HBSS. Rinse the testes with HBSS to remove blood and connective tissue. Finely mince the testes using sterile scissors in a clean Petri dish. Digest the minced tissue with collagenase type IV (1 mg/mL in DMEM/F-12) at 37 °C for 20-30 min. Neutralize the collagenase, centrifuge the mixture at a low speed $(300 \times g)$ for 5 min, discard the supernatant, and resuspend the pellet in DMEM/F- 12 supplemented with FBS (10%). Plate the cell suspension onto poly-L-lysine-coated culture dishes and incubate at 37 °C with 5% CO2 and 95% humidity. After 3 h, remove non-adherent cells (primarily germ cells and interstitial cells) by washing three times with pre-warmed DMEM/F- 12. Add fresh DMEM/F-12 with FBS (10%) to the adherent cells and continue the incubation. Perform media changes every 48 h until confluency is achieved. Cells were confirmed to be Sertoli cells by immunofluorescence staining for SOX9 and GATA4.

C18 -4 cells were grown in DMEM high glucose supplemented with 10% fetal bovine serum (FBS) and 1% Penicillin-Streptomycin Liquid. TM4 cells were grown in DMEM high glucose supplemented with 10% FBS and 1% Penicillin-Streptomycin Liquid. The expression plasmids encoding WT-GNA13 (NM_010303.3) (pCMV-HA-GNA13 and pCAG-GFP-GNA13) were constructed. The variant (C14S, C18S, C329S) was introduced into the WT-GNA13 plasmid using the MutExpress MultiS Fast Mutagenesis Kit (Vazyme, C215) following the manufacturer's instructions. Knockdown of GNA13 expression using siRNA. The information about siRNA and plasmids involved in this experiment is shown in Table S3. Transfection of the plasmids into cell lines was performed using Lipofectamine 3000 Reagent according to the manufacturer's protocol.

Isolation and characterization of exosomes derived from mouse sertoli cells

Mouse Sertoli cells were cultured in DMEM/F12 supplemented with 12% KnockOut SR Medium and 1% penicillin–streptomycin solution. After 48 h of incubation at 34 °C and 5% CO2, the supernatant was collected. EVs were isolated from cell culture supernatants using differential

ultracentrifugation as per MISEV guidelines. Briefly, media were sequentially centrifuged at 300 \times g at 4 °C for 10 min to remove cells, 2,000 \times g at 4 °C for 20 min to eliminate large debris, and 10,000 \times g at 4 °C for 20 min to pellet apoptotic bodies. Finally, EVs were pelleted at 120,000 \times g at 4 °C for 2 h and washed once with PBS under identical conditions. The supernatant was filtered through a 0.22 μm filter. The filtered liquid was then transferred to ultracentrifuge tubes and centrifuged at 120,000 \times g at 4 °C for 2 h. After discarding the supernatant, the pellet was resuspended in PBS and centrifuged at 120,000 \times g at 4 °C for 1 h. The supernatant was discarded, and the pellet was resuspended in 50–100 μL of PBS and stored at -80 °C for further use.

In this study, we employed scanning electron microscopy (SEM) and nanoparticle tracking analysis to comprehensively characterize exosomes. For SEM analysis, exosome samples were fixed, dehydrated, coated with a conductive material, and capturing images to visualize their morphology and surface characteristics. Nanosight NS300 was utilized to determine exosome size distribution and concentration by recording the Brownian motion of exosomes.

MDC staining

Monodansylcadaverine (MDC), an autofluorescent dye that selectively accumulates in acidic autophagic vacuoles, was used to visualize autophagosome formation. C18 -4 cells, a mouse spermatogonial cell line, were plated in a 6-well plate with 1 mL of MDC staining solution added to each well. The plate was then incubated at 37 °C in a light-avoiding cell culture incubator for 40 min. The MDC staining solution was aspirated, and the cells were washed three times with 1 mL of Assay Buffer. Finally, the cells were excited with ultraviolet light under a fluorescence microscope to observe green fluorescence.

Protein extraction western blot analysis

Wash the cells three times with PBS and extract total protein using RIPA lysis buffer. Separate a minimum of 15 µg of the sample on a 12% SDS-PAGE gel, then transfer it to a PVDF membrane. Block the membrane with 5% skim milk powder dissolved in tris-buffered saline with 0.1% Tween- 20 (TBST) for 1 h, followed by overnight incubation at 4 °C with the primary antibodies. Subsequently, incubate with horseradish peroxidase-conjugated goat anti-rabbit IgG (H +L) and horseradish peroxidase-conjugated goat anti-mouse IgG (H +L). Visualize the stained proteins using Immobilon Ultra-Plus Western HRP Substrate and normalize to β -Actin expression. Image analysis was performed using ImageJ 1.8.0 software.

Acyl-biotinyl exchange (ABE) assay

Cell lysis: TM4 cells were lysed in ice-cold lysis buffer for 30 min to extract total proteins while preserving post-translational modifications.

Blocking free thiols: To prevent non-specific labeling of non-palmitoylated cysteine residues, free thiols were irreversibly blocked by incubating lysates with 50 mM N-ethylmaleimide (NEM), a thiol-reactive alkylating agent, for 1 h at room temperature.

Protein precipitation: Samples were precipitated with cold acetone to remove excess NEM and concentrate proteins, followed by centrifugation at $14,000 \times g$ for 15 min at 4 °C.

Cleavage of thioester bonds: The protein pellet was resuspended in 1 M hydroxylamine (HAM, pH 7.4) to selectively hydrolyze thioester bond, thereby releasing palmitate and regenerating free thiols at previously palmitoylated sites. Control samples were treated with 1 M Tris–HCl (pH 7.4) instead of HAM to confirm the specificity of thioester cleavage.

Biotinylation: Newly exposed thiols were labeled with 0.2 mM Biotin-HPDP, a thiol-reactive biotinylation reagent, by incubating with streptavidin agarose beads for 2 h at room temperature. This step selectively tags palmitoylation sites.

Purification and detection: Biotinylated proteins were purified using streptavidin beads, eluted with SDS-PAGE loading buffer, and analyzed by immunoblotting with streptavidin-HRP to visualize palmitoylated proteins.

Acyl-PEG exchange (APE) assay

The APE assay was performed according to previous reports [55]. In brief, TM4 cells lysates were treated with 10 mM TCEP for 30 min. They were then incubated at room temperature with 50 mM NEM for 1 h to block free cysteine thiols. Proteins were precipitated using prechilled acetone. Subsequently, they were incubated with 1 M HAM at room temperature for 1 h. Finally, they were incubated with 1 mM mPEG-Mal (5 kDa) at room temperature for 2 h. Proteins were again precipitated using acetone, resuspended in 1× Laemmli buffer, boiled at 95 °C for 5 min, and separated by SDS-PAGE, followed by immunoblot analysis.

4D Label-free quantitative proteome analysis

We investigated the effects of 2-BP on the protein composition of EVs derived from mouse SCs using a proteomics approach. Primary mouse SCs were isolated and cultured in 10 cm dishes. When the cells reached 80% confluency, they were treated with 125 μM 2-BP for 24 h, using DMSO as a control group. The medium was then replaced with 12% KnockOut SR Medium, and the cells

were further cultured for 48 h to collect the cell supernatant. EVs in the cell supernatant were harvested using ultracentrifugation. Protein extraction and trypsin digestion were conducted, followed by LC–MS/MS. The Proteome Discoverer (v2.4.1.15) was used for MS/MS data analysis. FDR was adjusted to <1%.

Plasma membrane and intracellular membrane fractionation

In brief, transfer the cells and culture medium to a centrifuge tube and centrifuge at 500 ×g for 10 min at 4 °C. Discard the supernatant and add 10 mL of pre-chilled 1× PBS for washing. Centrifuge at 1000 x rpm for 5 min and repeat the wash twice. Add 1 mL of pre-chilled Buffer A to the collected cells or tissue and sonicate to lyse the cells, performing 3-4 cycles of 30 s each, with 1-min intervals in between, while keeping the samples on ice. Transfer the lysate to a pre-chilled centrifuge tube and centrifuge at 1000 ×g for 10 min at 4 °C to remove the pellet. Transfer the supernatant to a new pre-chilled centrifuge tube and centrifuge at 18,000 xrpm for 60 min at 4 °C. Transfer the resulting supernatant to a new tube for cytoplasmic proteins and store at - 80 °C. Add 500 μL of pre-chilled Buffer B to the pellet, vortex for 10 s, and incubate on ice for 30 min, vortexing intermittently 5–6 times. Centrifuge at $16,000 \times \text{rpm}$ for 10 min at 4 °C. Ouickly transfer the supernatant to a clean, pre-chilled microcentrifuge tube to obtain the membrane proteins. Aliquot and store at − 80 °C.

Co-immunoprecipitation (Co-IP)

C18 -4 cells underwent lysis using Western/IP lysis buffer for 30 min on ice. Subsequent centrifugation of the lysate occurred at 12,000 rpm and 4 °C for 15 min. The primary antibodies and Protein A+ G agarose was added into the supernatant, and samples were incubated overnight at 4 °C. The next day, the agarose was collected by centrifugation and washed five times with Western/IP lysis buffer. The beads were boiled for 15 min after resuspending in $1 \times SDS$ -PAGE loading buffer. BeyoMag Anti-HA Magnetic Beads (Beyotime, P2121) was used to precipitate exogenous HA-tag proteins, which did not form the heavy chain (HC) to interfere with other bands. The protein identification via mass spectrometry (MS) was performed by PTMBIO Co., LTD Hangzhou, China.

Immunofluorescence

In this study, we conducted immunofluorescence analysis in the C18 -4 cells and TM4 cells. Upon reaching the 80% confluency, the cells were fixed with 4% paraformaldehyde and permeabilized with Triton X- 100. A blocking step was conducted by incubating the cells with 5% bovine serum albumin (BSA) in PBS for 1 h at

37 °C. After blocking, the cells were incubated with the primary antibodies overnight at 4 °C. DAPI staining was employed to visualize the cell nuclei.

Statistical analysis

The results were analyzed by GraphPad (San Diego, CA) Prism 6.01 software. Data were analyzed using unpaired Student's t-test for two-group comparisons or one-way ANOVA followed by Tukey's post hoc test for multiple comparisons. A remarkable difference was considered statistically significant, which was presented as P < 0.05 (*) or P < 0.01 (**).

Abbreviations

GNA13 Guanine nucleotide binding protein, alpha 13 DHHC13 Zinc finger DHHC-type palmitoyltransferase 13

EVs Extracellular vesicles

SCs Sertoli cells

SSCs Spermatogonial stem cells PM Plasma membrane

ARHGEF12 Rho guanine nucleotide exchange factor 12

RhoA Ras homolog family member A PTMs Post-translational modifications

2-BP 2-Bromopalmitate HAM Hydroxylamine

Supplementary Information

The online version contains supplementary material available at https://doi.org/10.1186/s12964-025-02177-0.

Supplementary Material 1.

Supplementary Material 2.

Supplementary Material 3: Figure S1. Immunofluorescence distribution of the various GFP-proteins in TM4 cells treated with 125 μ M 2-BP. After transfecting GFP-LSM12, GFP-PPCS, GFP-ACTR3, GFP-YWHAZ, GFP-CUL1, GFP-CCS, GFP-CAPZB, GFP-GLT8D1, and GFP-G6PDX into TM4 cells for 24 hours, they were treated with 125 μ M 2-BP for 6 hours, with DMSO serving as the control group. Scale bar, 25 μ m.

Supplementary Material 4: Figure S2. SCs-derived EVs inhibits autophagy in spermatogonial stem cells. (A) Representative images of LC3II immunostaining of spermatogonia after EVs processing. (B) Representative images of MDA immunostaining of spermatogonia after EVs processing. Scale bar, 100 µm.

Supplementary Material 5: Figure S3. Efficiency validation of GNA13 expression vector and *GNA13*-siRNA in C18-4 cells. (A) Effect of HA-*GNA13* on relative *GNA13* mRNA expression was detected by RT-qPCR (*n* = 5). (B) Effect of *GNA13*-siRNA on relative *GNA13* mRNA expression was detected by RT-qPCR (*n* = 5). (C and D) Western blot analysis showing the expression of GNA13 when HA-*GNA13* and *GNA13*-siRNA were transfected into C18-4 cells.

Supplementary Material 6.

Supplementary Material 7.

Supplementary Material 8.

Acknowledgements

We thank Dr. Xandra O. Breakefield (Harvard Medical School) for providing CD513B-palm-mCherry plasmid.

Authors' contributions

DWZ performed the conceptualization. CHR and DWZ performed the data curation. GHH contributed to the experiments. DWZ and YSQ did the

supervision. CHR and GHH wrote the original draft. LY, LL, LSJ, JTQ, WY, GY, YSQ and DWZ reviewed and edited the manuscript. All authors agreed with the conclusion and approved the final version of manuscript.

Funding

This study was supported by the National Natural Science Foundation of China (Grant No. C1704 - 32172737), the National key research and development program of China (NO: 2023YFD130060103) and the China Postdoctoral Science Foundation (No. 2023M742727).

Data availability

No datasets were generated or analysed during the current study.

Declarations

Ethics approval and consent to participate

This study was approved by the Northwest A&F University, China.

Consent for publication

All authors have approved the manuscript and agree for the submission.

Competing interests

The authors declare no competing interests.

Received: 15 January 2025 Accepted: 26 March 2025 Published online: 09 April 2025

References

- 1. O'Donnell L, Smith LB, Rebourcet D. Sertoli cells as key drivers of testis function. Semin Cell Dev Biol. 2022;121:2–9.
- Silva AM, Lázaro-Ibáñez E, Gunnarsson A, Dhande A, Daaboul G, Peacock B, Osteikoetxea X, Salmond N, Friis KP, Shatnyeva O, et al. Quantification of protein cargo loading into engineered extracellular vesicles at singlevesicle and single-molecule resolution. J Extracell Vesicles. 2021;10(10): e12130.
- Takahashi Y, Takakura Y. Extracellular vesicle-based therapeutics: Extracellular vesicles as therapeutic targets and agents. Pharmacol Ther. 2023;242: 108352
- You Y, Tian Y, Yang Z, Shi J, Kwak KJ, Tong Y, Estania AP, Cao J, Hsu WH, Liu Y, et al. Intradermally delivered mRNA-encapsulating extracellular vesicles for collagen-replacement therapy. Nat Biomed Eng. 2023;7(7):887–900.
- Garcia-Martin R, Wang G, Brandão BB, Zanotto TM, Shah S, Kumar Patel S, Schilling B, Kahn CR. MicroRNA sequence codes for small extracellular vesicle release and cellular retention. Nature. 2022;601(7893):446–51.
- Ma Y, Ma QW, Sun Y, Chen XF. The emerging role of extracellular vesicles in the testis. Hum Reprod. 2023;38(3):334–51.
- Liang J, Li H, Mei J, Cao Z, Tang Y, Huang R, Xia H, Zhang Q, Xiang Q, Yang Y, et al. Sertoli cell-derived exosome-mediated transfer of miR-145-5p inhibits Leydig cell steroidogenesis by targeting steroidogenic factor 1. Faseb j. 2021;35(6): e21660.
- Tan XH, Gu SJ, Tian WJ, Song WP, Gu YY, Yuan YM, Li XS, Xin ZC, Kim SW, Guan RL, et al. Extracellular vesicles derived from human Sertoli cells: characterizations, proteomic analysis, and miRNA profiling. Mol Biol Rep. 2022;49(6):4673–81.
- Li Q, Li H, Liang J, Mei J, Cao Z, Zhang L, Luo J, Tang Y, Huang R, Xia H, et al. Sertoli cell-derived exosomal MicroRNA-486-5p regulates differentiation of spermatogonial stem cell through PTEN in mice. J Cell Mol Med. 2021;25(8):3950–62.
- Gao H, Cao H, Li Z, Li L, Guo Y, Chen Y, Peng G, Zeng W, Du J, Dong W, et al. Exosome-derived Small RNAs in mouse Sertoli cells inhibit spermatogonial apoptosis. Theriogenology. 2023;200:155–67.
- Kondo K, Harada Y, Nakano M, Suzuki T, Fukushige T, Hanzawa K, Yagi H, Takagi K, Mizuno K, Miyamoto Y, et al. Identification of distinct N-glycosylation patterns on extracellular vesicles from small-cell and non-smallcell lung cancer cells. J Biol Chem. 2022;298(6): 101950.
- 12. Chen C, Zheng H, Luo Y, Kong Y, An M, Li Y, He W, Gao B, Zhao Y, Huang H *et al*: SUMOylation promotes extracellular vesicle-mediated

- transmission of IncRNA ELNAT1 and lymph node metastasis in bladder cancer. J Clin Invest 2021, 131(8).
- Jung S, Lee S, Kim HJ, Kim S, Moon JH, Chung H, Kang SJ, Park CG. Mesenchymal stem cell-derived extracellular vesicles subvert Th17 cells by destabilizing RORyt through posttranslational modification. Exp Mol Med. 2023;55(3):665–79.
- Wang L, Cai J, Zhao X, Ma L, Zeng P, Zhou L, Liu Y, Yang S, Cai Z, Zhang S, et al. Palmitoylation prevents sustained inflammation by limiting NLRP3 inflammasome activation through chaperone-mediated autophagy. Mol Cell. 2023;83(2):281-297.e210.
- Zhou L, He X, Wang L, Wei P, Cai Z, Zhang S, Jin S, Zeng H, Cui J. Palmitoylation restricts SQSTM1/p62-mediated autophagic degradation of NOD2 to modulate inflammation. Cell Death Differ. 2022;29(8):1541–51.
- Shi C, Yang X, Liu Y, Li H, Chu H, Li G, Yin H. ZDHHC18 negatively regulates cGAS-mediated innate immunity through palmitoylation. Embo j. 2022;41(11): e109272.
- 17. Zhang Y, Dong D, Xu X, He H, Zhu Y, Lei T, Ou H. Oxidized high-density lipoprotein promotes CD36 palmitoylation and increases lipid uptake in macrophages. J Biol Chem. 2022;298(6): 102000.
- Lei Y, Zhang X, Xu Q, Liu S, Li C, Jiang H, Lin H, Kong E, Liu J, Qi S, et al. Autophagic elimination of ribosomes during spermiogenesis provides energy for flagellar motility. Dev Cell. 2021;56(16):2313-2328.e2317.
- Ge X, He Z, Cao C, Xue T, Jing J, Ma R, Zhao W, Liu L, Jueraitetibaike K, Ma J, et al. Protein palmitoylation-mediated palmitic acid sensing causes blood-testis barrier damage via inducing ER stress. Redox Biol. 2022;54: 102380.
- Wu Y, Zhang X, Zhang X, Liu S, Zhang J, Sun S, Zhao S, Wang Z, Cui Y, Huang X, et al. ZDHHC19 localizes to the cell membrane of spermatids and is involved in spermatogenesis†. Biol Reprod. 2022;106(3):477–86.
- Nanjappa MK, Hess RA, Medrano TI, Locker SH, Levin ER, Cooke PS. Membrane-Localized Estrogen Receptor 1 Is Required for Normal Male Reproductive Development and Function in Mice. Endocrinology. 2016;157(7):2909–19.
- Mariscal J, Vagner T, Kim M, Zhou B, Chin A, Zandian M, Freeman MR, You S, Zijlstra A, Yang W, et al. Comprehensive palmitoyl-proteomic analysis identifies distinct protein signatures for large and small cancer-derived extracellular vesicles. J Extracell Vesicles. 2020;9(1):1764192.
- 23. Romancino DP, Buffa V, Caruso S, Ferrara I, Raccosta S, Notaro A, Campos Y, Noto R, Martorana V, Cupane A, et al. Palmitoylation is a post-translational modification of Alix regulating the membrane organization of exosome-like small extracellular vesicles. Biochim Biophys Acta Gen Subj. 2018;1862(12):2879–87.
- 24. Xie F, Su P, Pan T, Zhou X, Li H, Huang H, Wang A, Wang F, Huang J, Yan H, et al. Engineering Extracellular Vesicles Enriched with Palmitoylated ACE2 as COVID-19 Therapy. Adv Mater. 2021;33(49): e2103471.
- 25. Yi Q, Huang M, Zhang X, Xu Z, Sun J, Wang S, Xu H, Du Z, Liu M. GNA13 inhibits glioblastoma metastasis via the ERKs/FOXO3 signaling pathway. Cell Signal. 2023;109: 110789.
- 26. Xu Y, Rong J, Duan S, Chen C, Li Y, Peng B, Yi B, Zheng Z, Gao Y, Wang K, et al. High expression of GNA13 is associated with poor prognosis in hepatocellular carcinoma. Sci Rep. 2016;6:35948.
- Chapuy B, Cheng H, Watahiki A, Ducar MD, Tan Y, Chen L, Roemer MG, Ouyang J, Christie AL, Zhang L, et al. Diffuse large B-cell lymphoma patient-derived xenograft models capture the molecular and biological heterogeneity of the disease. Blood. 2016;127(18):2203–13.
- 28. Hu Y, Xing J, Chen L, Guo X, Du Y, Zhao C, Zhu Y, Lin M, Zhou Z, Sha J. RGS22, a novel testis-specific regulator of G-protein signaling involved in human and mouse spermiogenesis along with GNA12/13 subunits. Biol Reprod. 2008;79(6):1021–9.
- Drucker A, Yoo BH, Khan IA, Choi D, Montermini L, Liu X, Jovanovic S, Younis T, Rosen KV. Trastuzumab-induced upregulation of a protein set in extracellular vesicles emitted by ErbB2-positive breast cancer cells correlates with their trastuzumab sensitivity. Breast Cancer Res. 2020;22(1):105.
- 30. Xia Z, Zhang X, Liu P, Zhang R, Huang Z, Li D, Xiao X, Wu M, Ning N, Zhang Q, et al. GNA13 regulates BCL2 expression and the sensitivity of GCB-DLBCL cells to BCL2 inhibitors in a palmitoylation-dependent manner. Cell Death Dis. 2021;12(1):54.

- Zhang M, Zhou L, Xu Y, Yang M, Xu Y, Komaniecki GP, Kosciuk T, Chen X, Lu X, Zou X, et al. A STAT3 palmitoylation cycle promotes T(H)17 differentiation and colitis. Nature. 2020;586(7829):434–9.
- De I, Sadhukhan S. Emerging Roles of DHHC-mediated Protein S-palmitoylation in Physiological and Pathophysiological Context. Eur J Cell Biol. 2018;97(5):319–38.
- Tu M, Miyamoto S. RHOA, a small G-protein, signals to mitophagy through regulation of PINK1 protein stability and protects cardiomyocytes against ischemia. Autophagy. 2023;19(6):1865–6.
- Ren T, Zheng B, Huang Y, Wang S, Bao X, Liu K, Guo W. Osteosarcoma cell intrinsic PD-L2 signals promote invasion and metastasis via the RhoA-ROCK-LIMK2 and autophagy pathways. Cell Death Dis. 2019;10(4):261.
- Thiageswaran S, Steele H, Voigt AL, Dobrinski I: A Role for Exchange of Extracellular Vesicles in Porcine Spermatogonial Co-Culture. Int J Mol Sci 2022, 23(9).
- Cocucci E, Meldolesi J. Ectosomes and exosomes: shedding the confusion between extracellular vesicles. Trends Cell Biol. 2015;25(6):364–72.
- 37. Bijlmakers MJ, Marsh M. The on-off story of protein palmitoylation. Trends Cell Biol. 2003;13(1):32–42.
- Zhao L, Zhang C, Luo X, Wang P, Zhou W, Zhong S, Xie Y, Jiang Y, Yang P, Tang R, et al. CD36 palmitoylation disrupts free fatty acid metabolism and promotes tissue inflammation in non-alcoholic steatohepatitis. J Hepatol. 2018;69(3):705–17.
- Solis GP, Kazemzadeh A, Abrami L, Valnohova J, Alvarez C, van der Goot FG, Katanaev VL. Local and substrate-specific S-palmitoylation determines subcellular localization of Gαo. Nat Commun. 2022;13(1):2072.
- Yu F, Qian Z: Mechanisms for regulation of RAS palmitoylation and plasma membrane trafficking in hematopoietic malignancies. J Clin Invest 2023, 133(12).
- 41. Chen QT, Zhang ZY, Huang QL, Chen HZ, Hong WB, Lin T, Zhao WX, Wang XM, Ju CY, Wu LZ, et al. HK1 from hepatic stellate cell-derived extracellular vesicles promotes progression of hepatocellular carcinoma. Nat Metab. 2022;4(10):1306–21.
- 42. Dong D, Yang J, Chen Y, Peng G, Cao H, Gao H, Jin T, Yang F, Dong W. Palmitoylated GLB1L4 transfers via exosomes to maintain sperm function in rat epididymis. Reproduction. 2021;161(2):159–72.
- 43. Wang M, Zeng L, Su P, Ma L, Zhang M, Zhang YZ. Autophagy: a multifaceted player in the fate of sperm. Hum Reprod Update. 2022;28(2):200–31.
- Hou F, Huang J, Qing F, Guo T, Ouyang S, Xie L, Ding Y, Yu J, Li Y, Liu X, et al. The rare-earth yttrium induces cell apoptosis and autophagy in the male reproductive system through ROS-Ca(2+)-Camkll/Ampk axis. Ecotoxicol Environ Saf. 2023;263: 115262.
- Mancilla H, Maldonado R, Cereceda K, Villarroel-Espíndola F, Montes de Oca M, Angulo C, Castro MA, Slebe JC, Vera JC, Lavandero S et al: Glutathione Depletion Induces Spermatogonial Cell Autophagy. J Cell Biochem 2015, 116(10):2283–2292.
- 46. Yang X, Song X, Li Z, Liu N, Yan Y, Liu B. Crosstalk between extracellular vesicles and autophagy in cardiovascular pathophysiology. Pharmacol Res. 2021;172: 105628.
- 47. Kuang Y, Zheng X, Zhang L, Ai X, Venkataramani V, Kilic E, Hermann DM, Majid A, Bähr M, Doeppner TR. Adipose-derived mesenchymal stem cells reduce autophagy in stroke mice by extracellular vesicle transfer of miR-25. J Extracell Vesicles. 2020;10(1): e12024.
- Cao J, Chen C, Chen Q, Gao Y, Zhao Z, Yuan Q, Li A, Yang S, He Y, Zu X, et al. Extracellular vesicle miR-32 derived from macrophage promotes arterial calcification in mice with type 2 diabetes via inhibiting VSMC autophagy. J Transl Med. 2022;20(1):307.
- Li G, Wang B, Ding X, Zhang X, Tang J, Lin H. Plasma extracellular vesicle delivery of miR-210-3p by targeting ATG7 to promote sepsis-induced acute lung injury by regulating autophagy and activating inflammation. Exp Mol Med. 2021;53(7):1180–91.
- Tu M, Tan VP, Yu JD, Tripathi R, Bigham Z, Barlow M, Smith JM, Brown JH, Miyamoto S. RhoA signaling increases mitophagy and protects cardiomyocytes against ischemia by stabilizing PINK1 protein and recruiting Parkin to mitochondria. Cell Death Differ. 2022;29(12):2472–86.
- You JS, Kim Y, Lee S, Bashir R, Chen J. RhoA/ROCK signalling activated by ARHGEF3 promotes muscle weakness via autophagy in dystrophic mdx mice. J Cachexia Sarcopenia Muscle. 2023;14(4):1880–93.
- Belaid A, Ndiaye PD, Cerezo M, Cailleteau L, Brest P, Klionsky DJ, Carle GF, Hofman P, Mograbi B. Autophagy and SQSTM1 on the RHOA(d) again:

- emerging roles of autophagy in the degradation of signaling proteins. Autophagy. 2014;10(2):201–8.
- Preau S, Delguste F, Yu Y, Remy-Jouet I, Richard V, Saulnier F, Boulanger E, Neviere R. Endotoxemia Engages the RhoA Kinase Pathway to Impair Cardiac Function By Altering Cytoskeleton, Mitochondrial Fission, and Autophagy. Antioxid Redox Signal. 2016;24(10):529–42.
- Amiri N, Mohammadi P, Allahgholi A, Salek F, Amini E. The potential of sertoli cells (SCs) derived exosomes and its therapeutic efficacy in male reproductive disorders. Life Sci. 2023;312: 121251.
- Percher A, Ramakrishnan S, Thinon E, Yuan X, Yount JS, Hang HC. Mass-tag labeling reveals site-specific and endogenous levels of protein S-fatty acylation. Proc Natl Acad Sci U S A. 2016;113(16):4302–7.

Publisher's Note

Springer Nature remains neutral with regard to jurisdictional claims in published maps and institutional affiliations.